AIP | Physics of Plasmas

Indirect determination of the electric field in plasma discharges using laser-induced fluorescence spectroscopy

J. Vaudolon and S. Mazouffre

Citation: Physics of Plasmas (1994-present) **21**, 093505 (2014); doi: 10.1063/1.4895532
View online: http://dx.doi.org/10.1063/1.4895532
View Table of Contents: http://scitation.aip.org/content/aip/journal/pop/21/9?ver=pdfcov
Published by the AIP Publishing

Indirect determination of the electric field in plasma discharges using laser-induced fluorescence spectroscopy

J. Vaudolon[a] and S. Mazouffre[b]
CNRS - ICARE (Institut de Combustion Aérothermique Réactivité et Environnement), 1 C Av. de la Recherche Scientifique, 45071 Orléans Cedex 2, France

(Received 18 June 2014; accepted 1 September 2014; published online 15 September 2014)

The evaluation of electric fields is of prime interest for the description of plasma characteristics. In this work, different methods for determining the electric field profile in low-pressure discharges using one- and two-dimensional Laser-Induced Fluorescence (LIF) measurements are presented and discussed. The energy conservation, fluid, and kinetic approaches appear to be well-suited for the electric field evaluation in this region of the plasma flow. However, the numerical complexity of a two-dimensional kinetic model is penalizing due to the limited signal-to-noise ratio that can be achieved, making the computation of the electric field subject to large error bars. The ionization contribution which appears in the fluid model makes it unattractive on an experimental viewpoint. The energy conservation and 1D1V kinetic approaches should therefore be preferred for the determination of the electric field when LIF data are used. © *2014 AIP Publishing LLC*.
[http://dx.doi.org/10.1063/1.4895532]

I. INTRODUCTION

The electric field distribution plays a fundamental role in the dynamics, the physical processes, and the organization of plasma discharges. It governs the species transport, wave structures, ionization phenomena, and sheath properties and its precise determination is therefore a key.[1–4] Different techniques have been developed to measure macro- and micro-fields in low-pressure discharges. Intrusive methods such as Langmuir and emissive probes are widely used.[5,6] A Langmuir probe can provide the plasma potential with a reasonable uncertainty. An emissive probe is a quick and easy way to access the local plasma potential using the floating point technique, provided the sheath potential is significantly reduced to limit the error on the measurement.[7] More sophisticated methods are available for properly extracting the plasma potential from the current-voltage trace.[8] Langmuir and emissive probes, however, suffer from a variety of intricate uncertainties, such as the theory used to derive the plasma quantities, contamination issues, and their inherent intrusive nature.

In contrast, optical methods have the advantage of being non-intrusive. Unlike probes, optical techniques also do not require complex apparatus to compensate for the strong oscillations of the discharge. The Stark effect of high Rydberg states of the hydrogen, helium, argon, krypton, and xenon gases has been successfully measured by a technique called fluorescence dip spectroscopy, with high spatial and temporal resolution.[9–13] In short, this technique excites ions from their ground state to a short-lived intermediate state with one or two photons coming from a first laser. The fluorescence light from this intermediate state is then depleted when a second step excitation is resonant with a Rydberg state. In highly excited Rydberg states, the electrons are on large orbits and the electric field of the core is relatively weak. Thus, small external fields can be detected with a great accuracy. The minimum detectable field is mostly limited by the finite bandwidth of the laser radiation and is on the order of 1 V/cm.[13] Fluorescence dip spectroscopy is accurate but cumbersome and expensive since it requires solid-state lasers and complex optical trains.

Laser-Induced Fluorescence (LIF) on a metastable ion state is affordable with laser diodes and is less complicated, provided that the metastable state properties can describe the ground state dynamics. This technique has been extensively used over the past several years in low-pressure cross-field discharges.[14] The basic idea of LIF is to access the velocity of probed particles along a CW laser beam direction by measuring the Doppler shift of absorbed photons. This technique allows the direct measurement of the ion velocity distribution function (IVDF) since the laser bandwidth is much narrower than the Doppler width. LIF has high spatial and temporal resolution.[18] The determination of the local electric fields, however, is indirect and requires the use of a physical model. The purpose of this paper is to evaluate the applicability of different models for computing the electric field distribution from LIF measurements in low-pressure plasma discharges. The Hall thruster plasma source, dedicated to space propulsion, is used in this study. Some of the processes that appear in these discharges remain poorly understood, despite decades of research.[19] The properties of these discharges (the complex cross-field topology, the kinetic regime of the plasma and the partial overlapping of the ionization and acceleration zones) make their use interesting in light of this study. Such sources have been extensively characterized in the past using LIF, but many studies only report one-dimensional (1D) LIF.[14] LIF measurements can require several weeks of experiments for the derivation of a full electric field profile. For this reason, the choice of the physical model which best describes the problem at stake and an evaluation

[a]julien.vaudolon@cnrs-orleans.fr
[b]stephane.mazouffre@cnrs-orleans.fr

of the practical possibilities for reducing the number of acquisitions is an important issues.

The plasma source is shown in Fig. 1. The electric and magnetic field directions are given. The measurements have been performed on the cavity axis (red line). The laser wave vector used for the LIF measurements is designated as **k**. We use an (r, θ, z) cylindrical coordinate system to account for the annular shape of the source. Azimuthal contributions are neglected.

Section II introduces the LIF technique principles and the theoretical models that can be used to derive the electric field profile from LIF measurements. Section III describes the plasma discharge, the LIF optical train, and the experimental procedure. Results are analyzed and discussed in Sec. IV. Finally, conclusions and recommendations are discussed in Sec. V.

II. POSSIBLE EXPERIMENTAL METHODS FOR DETERMINING THE E FIELD PROFILE USING LIF DATA

LIF spectroscopy is a non-intrusive diagnostic tool that allows the determination of the velocity of probed particles along a CW laser beam direction through measurement of the Doppler shift of absorbed photons.[14–17] Ions at velocity **v** with an electronic transition frequency Ω_0 may be driven to an excited state provided they satisfy the required Doppler shift

$$\Omega_L - \mathbf{k_L}.\mathbf{v} = \Omega_0, \tag{1}$$

where Ω_L is the shifted frequency and $\mathbf{k_L}$ is the laser wave vector. Scanning the laser frequency yields the one-dimensional distribution function. As indicated by the above equation, ion velocity components along the two axes perpendicular to $\mathbf{k_L}$ are not preferentially selected by the laser. Thus, the measured distribution is

$$f(\mathbf{x}, v_z, t) = \int\int f(\mathbf{x}, \mathbf{v}, t) d^2\mathbf{v}, \tag{2}$$

where we have taken the laser beam to be along the z direction to match the description in Fig. 1. Typical axial and radial IVDF measurements along the channel axis at 4 mm downstream the exit plane can be seen in Fig. 3.

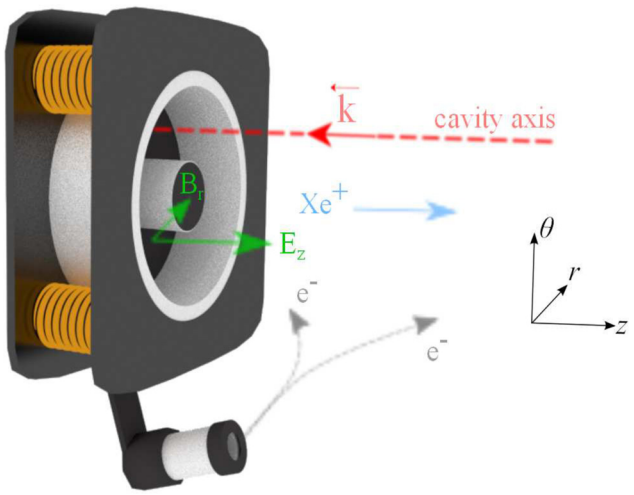

FIG. 1. Layout of the cross-field ion source; **k** is the laser wave vector.

Time-averaged and time-resolved LIF have been widely used to measure the characteristics of the electric field in low-pressure cross-field discharges.[14,20–22] Ion velocity measurements using LIF are extremely accurate, being limited only by the wave-meter resolution. Depending on the selected atom and optical transition, the line broadening due to the Zeeman effect can also be accounted for in order to increase the IVDF resolution. Since LIF measures the ion velocity instead of the local plasma potential as an emissive probe does, a direct evaluation of the ion kinetic energy is made. An appropriate physical model is, however, required in order for the electric field to be computed. Nevertheless, the IVDF is a fundamental quantity that provides additional information regarding the thermodynamic state of the system. The energy conservation and the fluid and Boltzmann models that have been considered in the present work are now described.

A. Energy conservation

Since the ionization and acceleration regions partially overlap in a Hall thruster, the locally created ions, with a null mean velocity, also contribute to the overall mean velocity value of the IVDF. Using the ion mean velocity (first order moment of the IVDF) will therefore result in an underestimation of the true local axial electric field. The simplest way to evaluate the electric field using a LIF data set is to compute the ion potential energy using the most probable ion velocity. Ions with this velocity have been generated at the beginning of the ionization zone where no acceleration is experienced. The most probable ion velocity group subsequently flows out of the entire acceleration domain at the measurement point. The evaluation of the potential then simply reduces to the energy conservation equation for a particle in a static electric field. This viewpoint differs from an ensemble average perspective reached when considering the ion mean velocity. Use of this quantity is further addressed in the fluid model. Under these considerations, the energy conservation therefore reads

$$\frac{1}{2} m_i v^2 = eU, \tag{3}$$

where notations have their usual meaning. Section III C provides details about our measurements and particularly sheds light on the fact that we neglect the mixed spatial derivatives. The radial and axial accelerating electric fields thus read

$$\begin{aligned} E_r &= \frac{m_i}{2e}\frac{dv_r^2}{dr}, \\ E_z &= \frac{m_i}{2e}\frac{dv_z^2}{dz}, \end{aligned} \tag{4}$$

where, in this case, v_r and v_z, respectively, refer to the radial and axial most probable ion velocities.

B. Fluid equations

We first consider the steady-state continuity and momentum conservation equations for unmagnetized ions, in the case of negligible charge-exchange and momentum-exchange collisions, which give

$$\begin{cases} \nabla.(n\mathbf{w_1}) = \nu_i n, \\ \nabla.(n\mathbf{w_1} \otimes \mathbf{w_1}) = \dfrac{e}{m_i} n\mathbf{E} + \nu_i n\mathbf{u_n} - \dfrac{1}{m_i}\nabla\mathbf{P}, \end{cases} \tag{5}$$

where n is the plasma density, ν_i is the ionization frequency, $\mathbf{u_n}$ is the neutral velocity, $\mathbf{w_1} = (w_{1,r}, w_{1,z})$ is the ion mean velocity, which is given by the first order moment of the IVDF, and $\mathbf{P}$ is the pressure tensor. No strong shear stresses are expected in this region of the ion flow. Off diagonal elements of the pressure tensor are therefore set to zero. The collisionless medium and the strong anisotropy of the plasma flow, however, imply to distinguish the radial and axial pressure terms. The continuity equation is inserted in the momentum balance equation which leads to contribution to the electric field by a term containing the ionization frequency and the ion flow velocity. The term containing the neutral velocity is neglected here since the neutral flow is assumed to be zero. The one dimensional case has only been studied since our analysis does not consider the mixed spatial derivatives (see Sec. III C for the experimental procedure). The electric fields thus read

$$\frac{eE_r}{m_i} = w_{1,r}\frac{dw_{1,r}}{dr} + \nu_i w_{1,r} + \frac{1}{nm_i}\frac{dP_{rr}}{dr}, \tag{6}$$

$$\frac{eE_z}{m_i} = w_{1,z}\frac{dw_{1,z}}{dz} + \nu_i w_{1,z} + \frac{1}{nm_i}\frac{dP_{zz}}{dz}. \tag{7}$$

The ionization and pressure gradient terms need to be considered for the electric field profile to be computed. However, measuring these terms is a complicated task. In order to distinguish the acceleration and ionization contributions, the Boltzmann equation can be used.

C. Boltzmann equation

The Boltzmann equation uses the IVDF directly inferred from LIF measurements. Neglecting charge-exchange collisions, momentum-exchange collisions, and the neutral gas temperature compared to the ion energy, the Boltzmann equation reads

$$\mathbf{v}.\nabla_\mathbf{r} f + \mathbf{a}.\nabla_\mathbf{v} f = \nu_i f_0, \tag{8}$$

where $\nabla_\mathbf{r}$ and $\nabla_\mathbf{v}$ stand for the space and velocity gradients, $\mathbf{a}$ is the acceleration, and f_0 is the distribution of the neutrals, approximated by a Dirac delta function.[23] The use of the Boltzmann equation has two main advantages. First, it considers the kinetic nature of the plasma processes. Second, the ionization and acceleration terms can be evaluated independently, even though these processes appear to be intimately linked in the discharge.

The 1D1V expression of the axial electric field has been developed by Pérez-Luna *et al.*[23] and reads

$$\frac{eE_z}{m_i} = \frac{w_1 w_2}{2w_1 - w_3}\frac{dw_3}{dz}, \tag{9}$$

where

$$\begin{cases} u_m = \dfrac{\int v_z^m f dv_z}{\int f dv_z} \\ w_m = \dfrac{u_m}{u_{m-1}},\ m \geq 2,\ w_1 = u_1\,. \end{cases} \tag{10}$$

Similarly, we propose to derive the radial 1D1V expression

$$\frac{eE_r}{m_i} = \frac{w_1 w_2}{2w_1 - w_3}\frac{dw_3}{dr}, \tag{11}$$

w_i in this radial case has been evaluated by the integration of the radial velocity components with their respective distributions.

The 2D2V radial and axial electric field expressions have been derived by Spektor.[22] Adopting the notation introduced by Pérez-Luna *et al.*,[23] we define

$$\begin{cases} u_{i,r}u_{j,z} = \dfrac{\int\int v_r^i v_z^j f dv_r dv_z}{\int\int f dv_r dv_z} \\ w_{m,l} = \dfrac{u_{m,l}}{u_{m-1,l}}, \end{cases} \tag{12}$$

where $l = r, z$. In order to simplify the electric field expressions, we use the notation introduced by Spektor.[22] Let us write

$$\begin{cases} z_r = \dfrac{\xi_2\gamma_1 + \gamma_2}{1 - \xi_1\xi_2} \\ z_z = \dfrac{\xi_1\gamma_2 + \gamma_1}{1 - \xi_1\xi_2} \\ \xi_1 = -\dfrac{w_{1,r}}{w_{3,z}}\dfrac{2w_{1,z} - w_{2,z}}{2w_{1,z} - w_{3,z}} \\ \xi_2 = -\dfrac{w_{1,z}}{w_{3,r}}\dfrac{2w_{1,r} - w_{2,r}}{2w_{1,r} - w_{3,r}} \\ \gamma_1 = \dfrac{dw_{3,z}/dz}{2w_{2,z} - w_{3,z}} - \dfrac{1}{w_{2,z}}\dfrac{2w_{1,z} - w_{2,z}}{2w_{1,z} - w_{3,z}}\dfrac{dw_{1,r}}{dr} \\ \qquad - \dfrac{dw_{1,z}w_{2,z}/dz}{w_{1,z}w_{2,z}} \\ \gamma_2 = \dfrac{dw_{3,r}/dr}{2w_{2,r} - w_{3,r}} - \dfrac{1}{w_{2,r}}\dfrac{2w_{1,r} - w_{2,r}}{2w_{1,r} - w_{3,r}}\dfrac{dw_{1,z}}{dz} \\ \qquad - \dfrac{dw_{1,r}w_{2,r}/dr}{w_{1,r}w_{2,r}}. \end{cases} \tag{13}$$

The electric field expressions therefore read

$$\frac{eE_r}{m_i} = \frac{w_{1,r}w_{2,r}}{2w_{1,r} - w_{3,r}}\frac{dw_{3,r}}{dr} + \frac{w_{2,r} - w_{3,r}}{2w_{1,r} - w_{3,r}}\left(z_r w_{1,r}w_{1,z} + w_{1,r}\frac{dw_{1,z}}{dz}\right), \tag{14}$$

$$\frac{eE_z}{m_i} = \frac{w_{1,z}w_{2,z}}{2w_{1,z} - w_{3,z}}\frac{dw_{3,z}}{dz} + \frac{w_{2,z} - w_{3,z}}{2w_{1,z} - w_{3,z}}\left(z_r w_{1,r}w_{1,z} + w_{1,z}\frac{dw_{1,r}}{dr}\right). \tag{15}$$

The ionization frequency can be written as

$$\nu_i = z_r w_{1,r} + z_z w_{1,z} + \frac{dw_{1,r}}{dr} + \frac{dw_{1,z}}{dz}. \tag{16}$$

The use of such expressions requires two-dimensional (2D) LIF measurements. Although the experimental determination of $f(\mathbf{x}, v_r, t)$ and $f(\mathbf{x}, v_z, t)$ is not an issue, measuring $f(\mathbf{x}, v_r, v_z, t)$

may be a time-consuming process. In Maxwellian plasmas, the assumption that $f(\mathbf{x}, v_r, v_z, t) = f(\mathbf{x}, v_r, t) \times f(\mathbf{x}, v_z, t)$ is valid as f is isotropic. In the particular source studied in this work, however, the on-channel axis radial IVDF is close to a Maxwellian distribution, while the axial IVDF departs from its initial Maxwellian shape due to several processes, the predominant contribution being the overlapping of the ionization and acceleration zones. The above field expressions nonetheless assume that the local 2D IVDF is the product of the radial and axial IVDFs. To account for the proper IVDF, one may use the optical tomography technique described by Koslover and McWilliams.[24] Tomography allows for the unambiguous determination of the complete ion velocity distribution using multiple 1D measurements on the velocity space. Computing the complete IVDF with this technique, however, requires the determination of a significative number of one dimensional IVDFs, resulting in a prohibitively long measurement period.

Notice that our 2D2V equations are not identical to those of Spektor.[22] Since only radial, respectively, axial, IVDFs have been measured at locations 1, 2, and 3, respectively, 2, 4, and 5, described in Sec. III C, we implicitly assumed that $\frac{dw_{(1,2),(r,z)}}{d(z,r)} \equiv 0$, resulting in the present simplified expressions.

III. EXPERIMENTAL SETUP

A. Plasma discharge

The Hall thruster used in this work has been extensively described in other studies.[25] A schematic of the source is shown in Fig. 1. In brief, it consists of a magnetic barrier in a low-pressure discharge maintained between an external cathode and an anode. The anode is located at the upstream end of a coaxial annular dielectric cavity that confines the discharge. The discharge electrons are magnetized, whereas the more massive ions are not. The high electron resistivity establishes a strong axial electric field that drives a fast azimuthal drift (the Hall current) responsible for the efficient ionization of the gas. This field also accelerates ions out of the discharge channel. As a direct consequence, the ionization and acceleration zones overlap. A fraction of the electrons emitted by the cathode neutralizes the ion beam. The term *exit plane* refers to the exit of the annular chamber.

The potential difference between the anode and the cathode is constant and equal to 200 V. The anode xenon mass flow rate is set at 1.0 mg/s, and the cathode mass flow rate fixed at 0.2 mg/s. Under these operating conditions, the discharge current mean value is 0.9 A. The experiments are performed in a stainless-steel vacuum chamber of 1.8 m long and 0.8 m in diameter. A background pressure of 2×10^{-5} mbars is achieved with a xenon mass flow rate of 1.0 mg/s and an input power of 250 W. The plasma source is mounted on two perpendicular linear translation stages to allow a displacement parallel and perpendicular to the source axis.

B. LIF optical train

The LIF optical assembly is described in detail in a review paper.[14] The $5d^4F_{7/2} \rightarrow 6p^4D_{5/2}$ Xe II transition is probed by an amplified tunable single-mode external cavity laser diode at 834.72 nm. The wavelength is accurately measured by a 60 m/s precision wave-meter. A high finesse Fabry-Perot interferometer is used to check the laser stability and detect mode-hops. An anamorphosis filter circularizes the laser beam. The primary laser beam is modulated by a mechanical chopper at a frequency $\sim$1 kHz before being coupled into a single-mode optical fiber of 5 μm core diameter. The laser beam propagates along the source axis and is aligned with the center of the discharge channel. The typical laser power density is 10 mW/mm^2 within the measurement volume, which guarantees a good signal-to-noise ratio and a limited saturation of the transition. A collection branch made of a 40 mm focal lens focuses the light onto a 200 μm core diameter optical fiber. Spatial resolution in the axial direction is 200 μm. The fluorescence light is focused onto the entrance slit of a 20 cm focal length monochromator that isolates the 541.9 nm line from the background. A photomultiplier tube serves as a light detector. For time-averaged LIF measurements, a lock-in amplifier operating at the chopper frequency is used to distinguish the fluorescence light from the intrinsic plasma emission.

C. Experimental procedure

The LIF data set includes 2D LIF measurements. The measurement points are sketched by a molecule whose central point is aligned on the cavity axis (see Fig. 1). The position $z = 0$ refers to the exit plane of the dielectric chamber of the source. This molecule is depicted in Fig. 2. Location 2 is moved to $z = 4$, 6, 8, 10, and 15 mm away from the exit plane. Radial measurements are performed at locations 1, 2, and 3, while axial IVDF has been acquired at locations 2, 4, and 5. Radial and axial spatial steps, namely, dr and dz, are both equal to 0.5 mm. This data set allows the evaluation of the axial and radial velocity gradients.

The isotopic and hyperfine line shapes have not been deconvolved from the IVDF profiles; this is at the origin of the small bump that can be observed at 3 km/s on the radial IVDF shown in Fig. 3.

IV. RESULTS AND DISCUSSIONS

In this section, we investigate the radial and axial electric field profiles obtained on the cavity axis through the application of different theories. The error bars which appear on the figures have been evaluated by adding a moderate level of white Gaussian noise to the LIF measurements. The

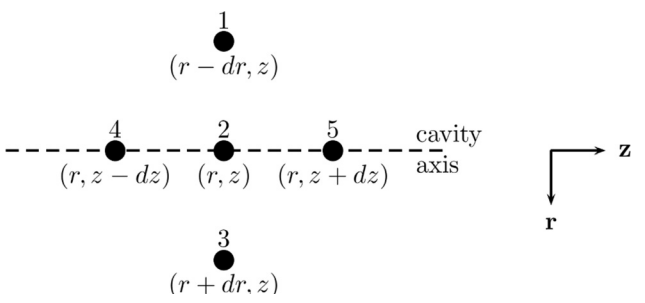

FIG. 2. Experimental measurement molecule. This molecule has been moved at 5 different locations along the channel axis.

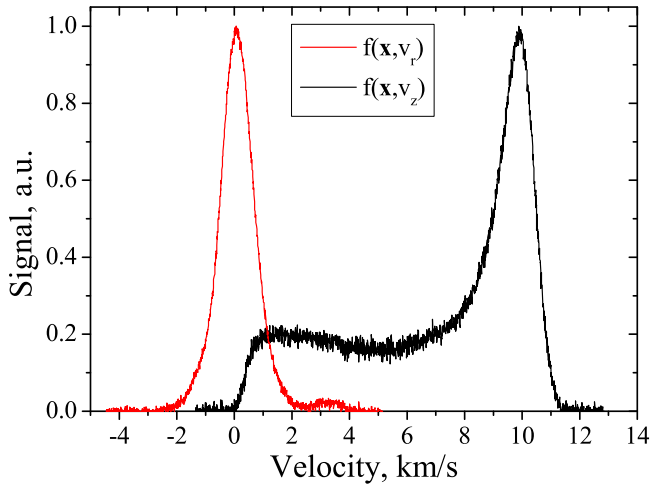

FIG. 3. Raw traces of the radial (in red) and axial (in black) time-averaged IVDFs at 4 mm downstream the exit plane.

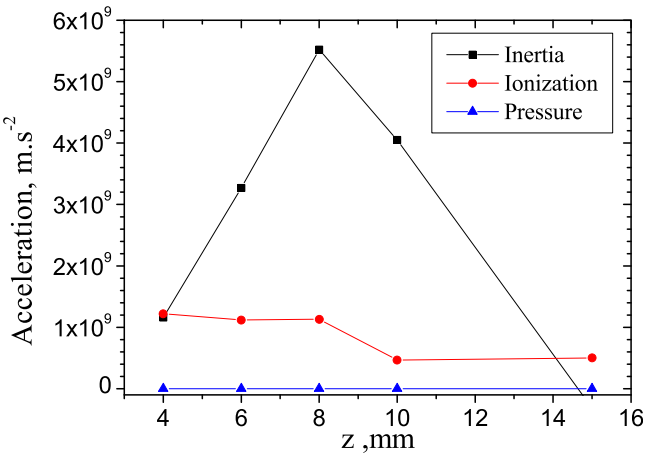

FIG. 4. Values of the inertial, ionization, and pressure terms which appear in the 1D axial fluid equation.

error bar amplitudes result from the comparison between the clean and noisy IVDF computations. The presented error bars represent the total error lower bound since the influence of the velocity uncertainty on the computations is not considered. Owing to the fact that only radial, respectively, axial, IVDFs have been measured at locations 1, 2, and 3, respectively, 2, 4, and 5, described in Sec. III C, we implicitly assumed that radial, respectively, axial, quantities do not vary axially, respectively, radially, considering that the (dr, dz) spatial steps are small enough for this assumption to be valid. Any azimuthal component contribution is neglected in the assumption of unmagnetized ions. Notice, however, that previous work on the same source revealed that a low azimuthal velocity component does exist.[26] The azimuthal velocity of the ions is driven not only by the magnetic deflection but the cathode influence must also be considered. For a more precise determination of the axial electric field, the azimuthal components must be taken into account.

Under these assumptions, the 2D radial and axial fluid equations reduce to their 1D expression. Since accessing the ionization frequency is a non-trivial task, this term is omitted in many experimental works. However, in a Hall thruster source, the ionization term is larger than the inertial term by approximately one order of magnitude at the beginning of the acceleration zone which is located inside the channel. The pressure term is similarly neglected in many studies. Fig. 4 presents the z evolution of the value of the inertial, ionization, and pressure gradient terms in the 1D axial fluid equation for our source. The inertial and ionization terms appear to be of similar importance. The pressure is, however, much lower by approximately 5 orders of magnitude. The ionization contribution therefore needs to be carefully evaluated.

The ionization frequency profile can be assessed using LIF and probe measurements, or using calibrated LIF alone, which then allows the determination of the ion density. One might think that fast measurements of the ionization frequency using probes (typically a few seconds with a fast translation stage) could be paired with the simple fluid model. The ion mean velocity used in the fluid model, however, requires the LIF measurement of the complete IVDF. For this reason, the electric field computation using a fluid approach is as demanding as using the kinetic approach. With the latter, the ionization and acceleration terms are evaluated separately. At low pressure, the fluid model is unsuitable for describing the ion flow which exhibits large Knudsen numbers. The fluid approach is therefore of little interest in an experimental work which aims at determining the **E** field profile at low pressure. At moderate Knudsen numbers, both kinetic and fluid methods are expected to provide similar results.

The energy conservation equation in which the most probable velocity is considered can be used to assess the electric field profile. This will result in the overestimation of local field, especially where the ionization and acceleration zones overlap, but the measurement time is greatly reduced since only the most probable ion velocity group is probed.

The Boltzmann equation is a powerful tool for computing the local electric field and ionization term. The independent evaluation of the accelerating electric field and the ionization frequency is possible under certain conditions.[23] The z 1D1V and (r, z) 2D2V equations have been used to compute the electric field and ionization frequency profiles. The w_i computations are extremely noise-sensitive and special care must be taken during the measurements to keep the final error bar as small as possible.

The results of the calculations are presented in Fig. 5. The outside peak in the electric field profile is clearly visible and distinguished by the four methods. The error bar tends to be larger with the 2D2V model, because of the finite signal-to-noise ratio and numerical errors. The field values are lower with the 2D2V computation since a small fraction of the total energy is lost in the radial component instead of being used for acceleration. The 3D3V model would further decrease the accelerating **E** field because of the ion azimuthal drift. The error bars globally tend to widen when the distance from the source increases due to the reduction in the signal-to-noise ratio level. Finally, the fluid model provides acceptable values of the electric field and reveals its structure. The regime of the ion flow can therefore be described using kinetic and fluid approaches, in this region at least.

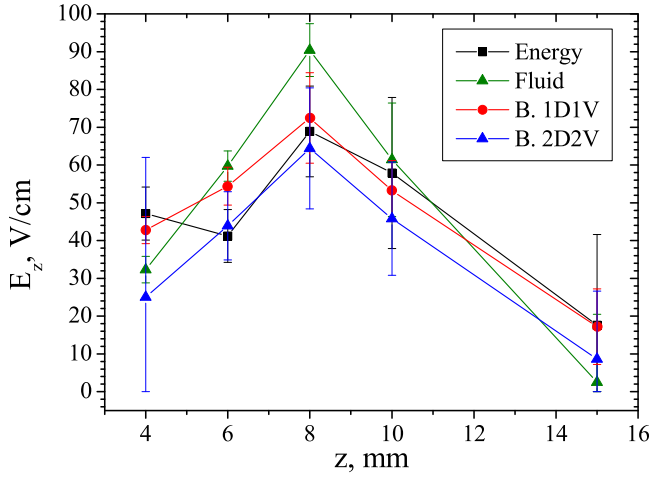

FIG. 5. Axial electric field profiles calculated with the energy conservation, the fluid, the Boltzmann 1D1V and 2D2V models.

The ionization frequency profile given in Fig. 6 has been computed using the two Boltzmann models presented in Sec. II C. Although the curve trends are similar, the 2D2V formulation leads to strong numerical constraints using experimental data and the error bar widens.

The radial electric field can be computed using the energy conservation and the 2D2V models. Since the ion velocity vector is purely axial on the channel axis, a zero net radial electric field is expected. However, as in the observations of Spektor,[22] the 2D2V Boltzmann equation leads to a non-zero radial electric field directed towards the source centerline. Similar to the study conducted in Ref. 22, we evaluate in Table I the *rr* and *zz* pressure tensor components contribution to the electric field values by computing $w_{2,(r,z)}/w_{1,(r,z)}$ since

$$u_{2,(r,z)} = u_{1,(r,z)}^2 + P_{(rr,zz)}. \tag{17}$$

From this expression, we can conclude that whenever the pressure tensor can be ignored $u_{2,(r,z)}/u_{1,(r,z)} \sim u_{1,(r,z)}$ and thus $w_{2,(r,z)} \sim w_{1,(r,z)}$. The pressure indeed plays an important role in the radial direction since the IVDF width is much

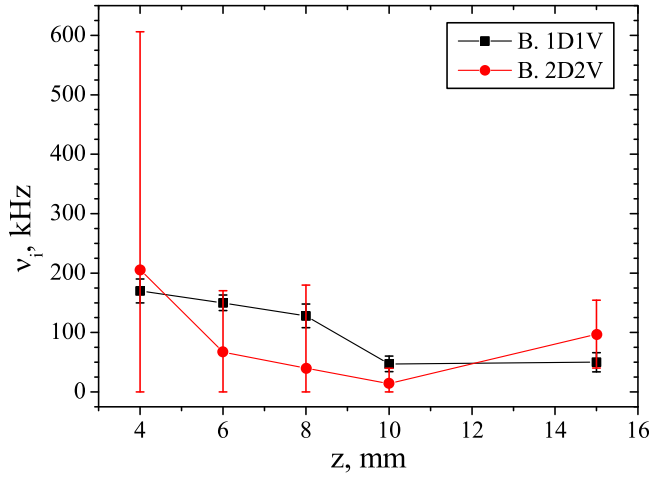

FIG. 6. Ionization frequency profile calculated using the Boltzmann 1D1V and 2D2V models.

TABLE I. Effect of the *rr* and *zz* pressure tensor components at various locations along the channel axis.

Z (mm)	4	6	8	10	15
$w_{2,z}/w_{1,z}$	1.19	1.17	1.14	1.10	1.14
$w_{2,r}/w_{1,r}$	32.8	7.59	163	9.30	2.21

larger than the ion radial mean velocity, but this may not be the reason for the observation of a radial electric field. The error bar associated with the E_r computation has been evaluated and ranges from 45 V/cm at 4 mm up to 150 V/cm at 10 mm. These values are well over the 6 V/cm that is computed by the 2D2V approach. Such an electric field would accelerate the ions towards a radial velocity of approximately 800 m/s on the *dr* step we used for the measurements. Depending on the axial position, radial velocities at location 1 range from 100 m/s to 300 m/s. These values are, however, coherent with the radial electric field values computed by the energy equation, which has been found to vary from −1 V/cm up to 3 V/cm. Notice that the same inability to produce coherent values of the radial electric field has been observed with the 1D1V Boltzmann radial equation. Azimuthal effects as well as distortion of the absorption line shape, due to the hyperfine structure and Zeeman effect, need to be considered for conclusive arguments to be made. The use of argon instead of xenon would be of interest in this matter since argon does not possess any abundant isotope, rendering the line profile simpler. However, the higher ionization potential of argon would lower the fluorescence signal and therefore decrease the signal-to-noise ratio.

V. CONCLUSIONS AND RECOMMENDATIONS

Several methods that can be used to derive the time-averaged axial electric field using LIF have been investigated. The fluid approach appears to be of very little interest in a very low pressure experimental work when ionization occurs locally but has been able to describe the intermediate ion flow regime of the source. The model's simplicity is, however, counterbalanced by the experimental requirements. The energy and Boltzmann equations can be used, provided special experimental and numerical care is taken. A trade-off between physical meaning and complexity makes the 1D1V Boltzmann equation preferable where ionization occurs. The ionization frequency can also be derived from the Boltzmann approach. The 2D2V formulation leads to a large error bar which makes the proper evaluation of the electric field profile and ionization term difficult. The radial electric field has also been calculated. Although its values were expected to be small, the 2D2V computation gives a non-zero radial field directed towards the source centerline, which is inconsistent with the zero mean ion radial velocities that have been measured. The large values of the error bar do not permit conclusions to be made concerning precise radial electric field values. The energy equation is, in this case, more suitable and provides meaningful results.

This work has been performed for time-averaged quantities. The time-resolved investigation is more complex, but it

may be of great interest for revealing the time-dependent balance between the different processes which together are used to describe the electric field profile. Time-resolved LIF has recently been successfully applied on low-pressure discharges using different techniques.[18,27,28] Accurately determining the temporal evolution of the electric field using LIF data, however, remains an open question.

ACKNOWLEDGMENTS

J. Vaudolon benefits from a CNES-Snecma Ph.D. grant.

[1]M. A. Lieberman and A. J. Lichtenberg, *Principles of Plasma Discharges and Materials Processing*, 2nd ed. (John Wiley and Sons, 2005).
[2]F. F. Chen, *Introduction to Plasma Physics*, 2nd ed. (Plenum Publishing Corporation, 1984).
[3]J.-M. Rax, *Physique des Plasmas* (Dunod, 2005).
[4]P. Chabert and N. Braithwaite, *Physics of Radiofrequency Plasmas* (Cambridge University Press, 2011).
[5]K. Dannenmayer and S. Mazouffre, "Electron flow properties in the far-field plume of a Hall thruster," Plasma Sources Sci. Technol. **22**, 035004 (2013).
[6]J. P. Sheehan and N. Hershkowitz, "Emissive probes," Plasma Sources Sci. Technol. **20**, 063001 (2011).
[7]J. Vaudolon and S. Mazouffre, "Evaluation of different methods for determining the electric field profile in a Hall thruster," in *Proceedings of the 4th Space Propulsion Conference, Germany* (2014).
[8]J. P. Sheehan, Y. Raitses, N. Hershkowitz, I. Kaganovitch, and N. J. Fisch, "A comparison of emissive probe techniques for electric potential measurements in a complex plasma," Phys. Plasmas **18**, 073501 (2011).
[9]U. Czarnetzki, D. Luggenhölscher, and H. F. Döbele, "Sensitive electric field measurement by fluorescence-dip spectroscopy of Rydberg states of atomic hydrogen," Phys. Rev. Lett. **81**, 4592 (1998).
[10]K. Dannenmayer and S. Mazouffre, "Space and time resolved electric field measurements in helium and hydrogen RF-discharges," Plasma Sources Sci. Technol. **8**, 230 (1999).
[11]K. Takizawa, K. Sasaki, and A. Kono, "Sensitive measurements of electric field distributions in low-pressure Ar plasmas by laser-induced fluorescence-dip spectroscopy," Appl. Phys. Lett. **84**, 185 (2004).
[12]T. Kampschulte, J. Schulze, D. Luggenhölscher, M. D. Bowden, and U. Czarnetzki, "Laser spectroscopic electric field measurement in krypton," New J. Phys. **9**, 18 (2007).
[13]U. Czarnetzki and K. Sasaki, "Ultra-sensitive measurement of sheath electric fields by laser-induced fluorescence-dip spectroscopy," J. Plasma Fusion Res. **83**, 215 (2007).
[14]S. Mazouffre, "Laser-induced fluorescence diagnostics of the cross-field discharge of Hall thrusters," Plasma Sources Sci. Technol. **22**, 013001 (2013).
[15]W. Demtröder, *Laser Spectroscopy: Basic Concepts and Instrumentation* (Springer, Berlin, 1998), p. 367.
[16]N. Sadeghi, "Molecular spectroscopy techniques applied for processing plasma diagnostics," J. Plasma Fusion Res. **80**, 767 (2004).
[17]I. A. Biloiu, E. E. Scime, and C. Biloiu, "One- and two-dimensional laser induced fluorescence at oblique incidence," Plasma Sources Sci. Technol. **18**, 025012 (2009).
[18]J. Vaudolon, L. Balika, and S. Mazouffre, "Photon counting technique applied to time-resolved laser-induced fluorescence measurements on a stabilized discharge," Rev. Sci. Instrum. **84**, 073512 (2013).
[19]V. V. Zhurin, H. R. Kaufman, and R. S. Robinson, "Physics of closed drift thrusters," Plasma Sources Sci. Technol. **8**, R1 (1999).
[20]S. Mazouffre and G. Bourgeois, "Spatio-temporal characteristics of ion velocity in a Hall thruster discharge," Plasma Sources Sci. Technol. **19**, 065018 (2010).
[21]J. Vaudolon, B. Khiar, and S. Mazouffre, "Time evolution of the electric field in a Hall thruster," Plasma Sources Sci. Technol. **23**, 022002 (2014).
[22]R. Spektor, "Computation of two-dimensional electric field from the ion laser induced fluorescence measurements," Phys. Plasmas **17**, 093503 (2010).
[23]J. Pérez-Luna, G. J. M. Hagelaar, L. Garrigues, and J. P. Boeuf, "Method to obtain the electric field and the ionization frequency from laser induced fluorescence measurements," Plasma Sources Sci. Technol. **18**, 034008 (2009).
[24]R. Koslover and R. McWilliams, "Measurement of multidimensional ion velocity distributions by optical tomography," Rev. Sci. Instrum. **57**, 2441 (1986).
[25]S. Mazouffre, G. Bourgeois, K. Dannenmayer, and A. Lejeune, "Ionization and acceleration processes in a small, variable channel width, permanent-magnet Hall thruster," J. Phys. D: Appl. Phys. **45**, 185203 (2012).
[26]G. Bourgeois, S. Mazouffre, and N. Sadeghi, "Unexpected transverse velocity component of Xe^+ ions near the exit plane of a Hall thruster," Phys. Plasmas **17**, 113502 (2010).
[27]C. J. Durot, A. D. Gallimore, and T. B. Smith, "Validation and evaluation of a novel time-resolved laser-induced fluorescence technique," Rev. Sci. Instrum. **85**, 013508 (2014).
[28]N. A. MacDonald, M. A. Capelli, and W. A. Hargus, Jr., "Time-synchronized continuous wave laser-induced fluorescence on an oscillatory xenon discharge," Rev. Sci. Instrum. **83**, 113506 (2012).